Desalination and Water Treatment
www.deswater.com

doi: 10.5004/dwt.2021.26901

217 (2021) 320–328
March

Efficient photocatalytic degradation of 2,4-dinitrophenol over mesoporous Zr and Ce co-doped TiO_2 under visible light

T. Usharani[a,b,*], R. Baskar[b], B. Palanisamy[c], M. Myilsamy[d]

[a]*Department of Chemical Engineering, Erode Sengunthar Engineering College, Perundurai 638 057, India, email: chemusharani@gmail.com (T. Usharani)*
[b]*Department of Food Technology, Kongu Engineering College, Perundurai 638 052, India, email: naturebaskar@yahoo.co.in*
[c]*Department of Chemistry, J.K.K. Nataraja College of Arts & Science, Komarapalayam 638 183, India, email: palanijkkn@gmail.com*
[d]*Department of Chemistry, Dr. N.G.P. Arts and Science College, Coimbatore 641048, India, email: myilsamy@drngpasc.ac.in*

Received 1 May 2020; Accepted 27 November 2020

ABSTRACT

In the present study, zirconium and cerium co-doped mesoporous TiO_2 photocatalysts were prepared by sol–gel technique using Pluronic P123 as the structure-directing agent. The prepared catalytic materials were characterized by X-ray diffraction, high-resolution transmission electron microscopy, N_2 sorption studies, diffuse reflectance UV-vis absorption spectroscopic analysis and X-ray photoelectron spectroscopy. Zirconium and cerium co-doping on TiO_2 induces visible-light absorption and decreases the bandgap energy. Zirconium and cerium co-doped mesoporous titania exhibit a high surface area with a large pore diameter. The photocatalytic activity has been evaluated for the photodegradation of 2,4-dinitrophenol under visible light illumination. The optimum loading of Zr^{4+} and Ce^{4+} to TiO_2 was found to be 0.5 wt.%. Ce^{4+} and Zr^{4+} active sites are good electron scavengers, which can easily trap the excited electrons and shift the electrons to the adsorbed oxygen molecules and therefore efficiently extending the lifetime of the electron-hole pair. Moreover, Zr^{4+}/Ce^{4+}-TiO_2 showed excellent photocatalytic activity towards the degradation of 2,4-dinitrophenol under visible light irradiation due to the formation of a large quantity of $^{\bullet}OH$ and $O_2^{-\bullet}$ radicals.

Keywords: Nanomaterials; Mesoporous; Zr^{4+}/Ce^{4+}-TiO_2; Photocatalytic degradation; 2,4-dinitrophenol

1. Introduction

Photodegradation of organic contaminants has been induced broad attention for both potential applications and scientific understanding due to greater environmental contamination in recent decades. Particularly, phenols are considered as a hazardous pollutant because of their potential to harm human health. The heterogeneous photocatalysis using TiO_2 as photocatalyst considered the most emerging technology for phenol degradation [1]. TiO_2 has been demonstrated as a promising universal photocatalyst owing to its superior photocatalytic efficiency, chemical and biological inertness, strong oxidizing ability, resistance to photo-corrosion, nontoxicity, and low cost [2–4]. However, titanium dioxide has disadvantages like the low capacity to utilize solar energy (not more than 5%) due to its broad bandgap and high rate of recombination of the photo-generated electron-hole pairs. In order to enhance the visible-light photocatalytic activity of TiO_2, various strategies such as doping with nonmetal [5–7] and metal [8–10] dye sensitization [11] and coupling with other semiconductors [12,13] have been reported to address these issues. Earlier studies have shown that doping of TiO_2 with other metal ions could be beneficial to shift the absorption capability of TiO_2 from UV to the visible light region (400–800 nm) [14–18]. It is reported that metal and non-metal ions doped

* Corresponding author.

mesoporous TiO_2 could effectively induce the visible light absorption, which occurs mainly excitation of smaller bandgap metal oxides and partially from the excitation of the introduced localized states in the bandgap of doped TiO_2 [19].

Among the various metal ion dopants, zirconium was found to be a suitable dopant for TiO_2 owing to its similar electronegativity, ionic radius and valence states which are beneficial sure to dope the preferred amount of Zr into TiO_2 without any defects [20]. For example, Gao et al. [21] reported that the Zr-loaded TiO_2 showed better catalytic efficiency than bare titanium dioxide for photodegradation of bisphenol A under visible-light illumination. Liu et al. [22] have prepared Zr incorporated TiO_2 nanotube clusters on the Ti sheets and the improved photocatalytic activity was studied. Goswami and Ganguli [23] explained the efficient photodegradation of quinalphos pesticide due to the bandgap modification of mesoporous TiO_2 by Zr doping.

In other words, it is reported that doping of lanthanide metal ions can produce defect levels in the bandgap, which traps the excited electrons easily and thereby increasing the lifetime of photo-generated charge carriers. In addition, these cerium ions doped oxides are identified to be excellent thermal stability because of their unique 4f electron configuration [24]. Among the lanthanide metal ions, cerium ions have considerable interest due to their high optical transparency in the visible region by Ce^{3+}/Ce^{4+} redox couple [25]. In general, cerium doped TiO_2 materials have been prepared by the hydrothermal and sol–gel methods and identified to improve the photodegradation of organic pollutants under visible light. Hence, most of the researchers have focused on preparing mesostructured cerium ions doped TiO_2 with vast surface area and convenient pore dimension to enhance the catalytic activity of titania. The doping of cerium ions (Ce^{3+}/Ce^{4+}) leads to enhance the number of defects or O_2 vacancies in the titanium dioxide crystal and also to increase the light absorption ability into the visible region [26]. The biggest advantage is that the photo-excited electrons trapped in Ce^{4+}/Ce^{3+} sites can be simply transferred to oxygen on the cerium introduced TiO_2 catalyst surface, which successfully restricts the rate of electron-hole recombination and hence enhanced the TiO_2 quantum yield. In recent years, co-doping of metal ions such as Ag and La [27], silver and V [28], Au and Ir [29], N and Ni [30], N and In [31], Sn and Zn [32], N and Zr [33], into semiconductor metal oxides have gained much attention because of its higher photocatalytic activity and unique optical and structural characteristics compared with the doping of one metal ion into semiconductor oxide.

In the present study, zirconium and cerium ions co-doped mesoporous TiO_2 was prepared by sol–gel process. The resultant photocatalyst showed the light absorption in the visible region and expected to increase the photocatalytic activity. The efficiency of the synthesized photocatalyst was evaluated by the photocatalytic degradation for 2,4-dinitrophenol under the illumination of visible light. Further, the optical properties of the photocatalysts and the photocatalytic mechanism was also explained in detail in the manuscript. To the best of our knowledge, zirconium and cerium ions co-doped mesoporous TiO_2 is a better photocatalyst for degradation for 2,4-dinitrophenol under the illumination of visible light.

2. Experimental

2.1. Materials

All the analytical grade reagents and chemicals were used without additional purification. Titanium(IV) isopropoxide (Merck, India), zirconyl nitrate (Merck, India) and cerium(III) nitrate hexahydrate (Merck, India) were used as the chemical sources for Ti, Zr and Ce respectively. Triblock copolymer (Pluronic P123, MW = 5800, $EO_{20}PO_{70}EO_{20}$; Aldrich), [poly(ethylene glycol)-block-poly(propylene glycol)-block-poly(ethylene glycol)] was used as a structure-directing agent. Double distilled water, pure ethanol (Merck, India) were utilized for the synthesis of the photocatalyst. The organic pollutant 2,4-dinitrophenol (Merck, India) was used for the photodegradation study.

2.2. Preparation of mesoporous bare TiO_2 and Zr^{4+}/Ce^{4+}-TiO_2

Mesoporous bare TiO_2 catalyst was prepared by sol–gel technique using Pluronic P123 as a structure-directing material with soft template mechanism. The preparation was carried out in a closed lid polypropylene bottle. 1 g of Pluronic P123 triblock copolymer was added into 32 mL of pure ethanol. Then stirring continued for another 4 h, a solution was attained in clear form. Titanium(IV) isopropoxide (3 mL) was added to the clear solution at ordinary room temperature and stirred another 2 h. Then water (18 mL) was added to the synthetic mixture and the stirring was continued at ordinary room temperature for 24 h. Afterwards, the obtained mixture was kept in dark for 12 h nucleation. The settled product was centrifuged in order to remove the template from the ethanol-water solution. In order to get fine catalyst powder, the solid precipitate was dried and powdered. This powder material was calcined nearly at 400°C in the nitrogen atmosphere for 6 h to eliminate the remaining structure-directing agent [34]. The prepared mesoporous bare TiO_2 catalyst was noted as meso-TiO_2. Three different wt.% of Zr and Ce incorporated TiO_2 were prepared in the same synthetic procedure by adding the stoichiometric quantity of zirconyl nitrate and cerium(III) nitrate hexahydrate as the Zr and Ce sources.

2.3. Catalyst characterization

The high angle X-ray diffraction patterns were recorded on the PANalytical X'Pert Pro X-ray diffractometer using CuKα radiation. The low angle X-ray diffraction patterns were analyzed on a Bruker D8 advanced powder X-ray diffractometer using CuKα (λ = 1.5418 Å) as the radiation source in the 2θ range 0.5°–6° with a step size of 0.01° and step time of 5 s. The N_2 sorption isotherms were analyzed by Micromeritics analyzer (ASAP 2020). Earlier to measurement, the samples were 3 h degassed at 300°C under vacuum (10^{-5} mbar) in the degas compartment of the adsorption analyzer. Surface area (specific) was measured by the Brunauer–Emmett–Teller technique and the distribution of pore dimension was measured using the Barrett–Joyner–Halenda technique. The morphology of prepared catalysts was studied by transmission electron microscopy (TEM) images were captured using a JEOL TEM-3010 electron microscope functioned at 300 keV accelerating voltage. X-ray photoelectron spectroscopy (XPS)

was recorded with MS Omicron nanotechnology using Monochromator XM-1000, K-alpha surface analyzer by AlKα as the source of radiation worked at 200 W semi-circular electron force analyzer. The DR UV-Vis spectra of the prepared catalysts were analyzed at the 200–800 nm range by Shimadzu UV-visible spectrophotometer (model 2450) with $BaSO_4$ as reference material. The Fourier-transform infrared (FTIR) spectroscopic studies were recorded by Nicolet Avatar 360 FTIR spectrometer with KBr pellet type technique.

2.4. Photocatalytic degradation studies and investigation

The catalytic activity of the prepared photocatalytic materials was examined by the photodegradation of aqueous 2,4-dinitrophenol (2,4-DNP) solution. Photodegradation was carried out in a slurry batch photocatalytic reactor under visible-light. A cylindrical photocatalytic reactor (2 cm diameter × 30 cm height) was used in all the experiments. The water circulation arrangement was used to maintain the reactor temperature range from 25°C to 30°C. A tungsten lamp (300 W) built into the reactor with polished aluminum reflectors was used as the source for visible-light and positioned near the reactor tube. These tungsten lamps emit only visible light above 400 nm wavelength.

In this experiment, 100 mg of the prepared catalyst was added to 100 mL aqueous 2,4-dinitrophenol solution of 30 ppm in a reaction glass tube. Earlier, the catalyst pollutant suspension ware stirred another 30 min without light conditions to achieve adsorption–desorption equilibrium. Then catalyst pollutant suspension exposed to visible-light above 410 nm wavelength with continuous purging of air with an air pump. At the definite instant, an aliquot of 5 mL of samples was withdrawn and to remove the catalytic particles centrifugation process followed by filtration (0.2 μm membrane) process was carried out. The photocatalytic degradation was investigated by identifying 2,4-DNP in wavelength of 358 nm by using the Elico SL218 double beam UV-Visible spectrophotometer. The amount of mineralization of 2,4-DNP was measured by (TOC) total organic carbon analyzer (Analytik Jena multi N/C 2100).

3. Results and discussion

3.1. Catalysts characterization

The low angle X-ray diffraction (XRD) patterns of meso-TiO_2, 0.5 wt.% Zr^{4+}-TiO_2, 0.5 wt.% Ce^{4+}-TiO_2, 0.1, 0.5 and 1 wt.% Zr^{4+}/Ce^{4+}-TiO_2 photocatalysts are presented in Fig. 1a. An intense reflection that occurred between 0.5° and 1° (2θ) reveals the presence of mesoporous structure in all materials. The higher angle XRD patterns of meso-TiO_2, 0.5 wt.% Zr^{4+}-TiO_2, 0.5 wt.% Ce^{4+}-TiO_2, 0.1, 0.5 and 1 wt.% Zr^{4+}/Ce^{4+}-TiO_2 are shown in Fig. 1b. All XRD patterns proved the existence of an anatase form of TiO_2 (JCPDS No. 21–1272). No characteristic diffraction peaks matching to Zr^{4+} and Ce^{4+} species were identified because of the lower concentration dopant metal. The possibility of CeO_2-TiO_2 solid solution was ignored because of the comparative large ionic size difference of Ce^{4+} cation (1.02 Å) with Ti^{4+} cation (0.68 Å). It is complicated for 8 coordinated cerium present to substitute 6 coordinated titanium in tetragonal TiO_2 [35]. Therefore, may be cerium ions vastly dispersed on the TiO_2 surface in the type of amorphous metal oxides. However, the doping of Zr^{4+}-ions are likely to occur in Ti^{4+} as the difference between the ionic boundary of the Ti^{4+} (0.68 Å) and Zr^{4+} (0.78 Å) is minute and therefore six coordinated Ti^{4+} can be replaced by six coordinated Zr^{4+}. As a result, the Zr^{4+} ions doping into titania lattice over the substitutional approach can be expected. Thus, it is reasonable to conclude that Zr^{4+} ions may be substituted into the TiO_2 lattice and Ce^{4+}-ions may exist in the form of amorphous metal oxides. The size of the prepared crystallite materials has been calculated using Scherrer's equation from the (101) crystal plane and the crystal sizes are 11.8, 10.6, 10.2, 9.4, 8.3 and 7.4 nm meant for meso-TiO_2, 0.5 wt.% Zr^{4+}-TiO_2, 0.5 wt.% Ce^{4+}-TiO_2, 0.1, 0.5 and 1 wt.% Zr^{4+}/Ce^{4+}-TiO_2 respectively. The dimension of particle

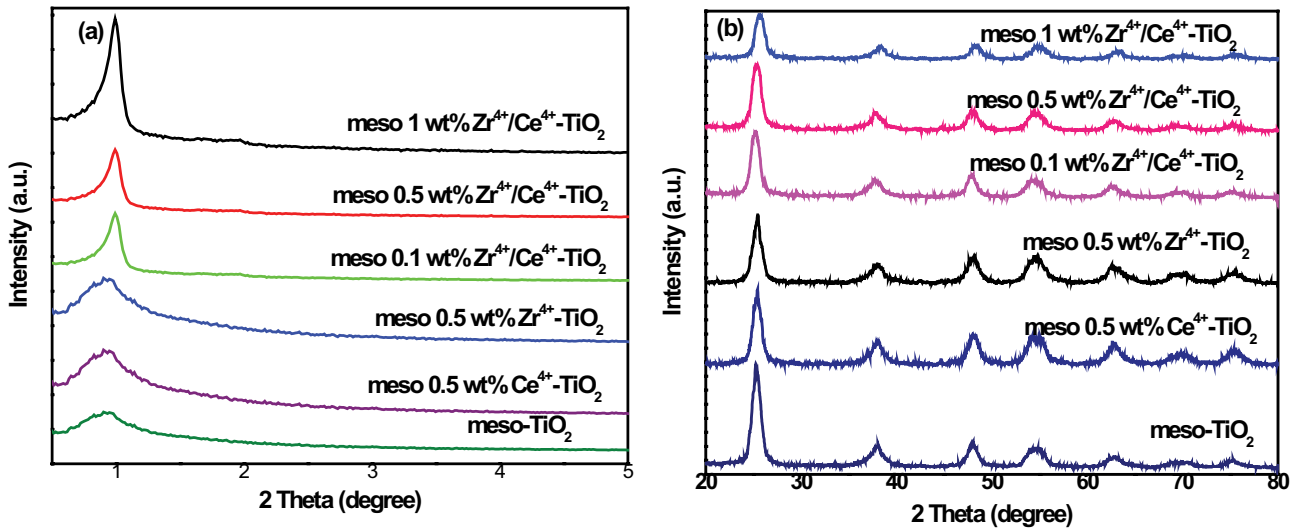

Fig. 1. (a) High angle XRD patterns of bare meso-TiO_2, 0.5 wt.% Zr^{4+}-TiO_2, 0.5 wt.% Ce^{4+}-TiO_2, 0.1, 0.5 and 1 wt.% Zr^{4+}/Ce^{4+}-TiO_2. (b) Low angle XRD patterns of bare meso-TiO_2, 0.5 wt.% Zr^{4+}-TiO_2, 0.5 wt.% Ce^{4+}-TiO_2, 0.1, 0.5 and 1 wt.% Zr^{4+}/Ce^{4+}-TiO_2.

reduced with an increase of the dopant metal concentration, because zirconium and cerium ions doping on TiO_2 lattice controlled the growth of crystallite of the TiO_2 nanoparticles.

The textural parameters of bare meso-TiO_2, 0.5 wt.% Zr^{4+}-TiO_2, 0.5 wt.% Ce^{4+}-TiO_2, 0.1, 0.5 and 1 wt.% Zr^{4+}/Ce^{4+}-TiO_2 photocatalysts were attained from N_2 sorption analyses are exhibited in Fig. 2. All the obtained isotherms reveal type IV adsorption isotherms with H_2 hysteresis loop at a higher relative pressure (p/p_0 = 0.8–0.9), which confirmed the characteristics of the mesoporous structure in all materials. The surface area (specific), pore diameter and pore capacity of prepared catalytic materials are exhibited in Table 1. The surface area enhances with an increase in co-metal ion doping till 0.5 wt.% and after decreases. Since the size of the particle reduces with an increase of dopant metal concentration, the surface area enhanced up to 0.5 wt.% co-doped TiO_2. At high dopant metal concentration, though grain size reduces, the well-dispersed Zr^{4+} and Ce^{4+} crystals on the TiO_2 surface block the active sites and hence the surface area of Zr^{4+}/Ce^{4+}-TiO_2 decreased above 0.5 wt.% loadings. It is well reported that a larger surface area and pore size can enhance the photocatalytic performance of the TiO_2 photocatalysts.

The high-resolution transmission electron microscopy images and selected area electron diffraction patterns of bare meso-TiO_2 and 0.5 wt.% Zr^{4+}/Ce^{4+}-TiO_2 photocatalysts were analyzed and exhibited in Fig. 3. The catalytic particles are nearly spherical in nature, and the grain size distributions are 5–12 nm range. These values are similar to the typical particle sizes calculated from X-ray diffraction patterns. The TEM image of 0.5 wt.% Zr^{4+}/Ce^{4+}-TiO_2 (Fig. 3d) shows the highly dispersed Zr^{4+} and Ce^{4+} ions on the TiO_2. The ultimate contact of Zr^{4+} and Ce^{4+} ions on TiO_2 is more advantageous to increase the interfacial electron transfer process. The Zr^{4+} and Ce^{4+} ions on TiO_2 undergo the interfacial charge transfer process increases significantly. The well-determined lattice fringes were observed in Figs. 3b and e, this explained the crystalline character of TiO_2 catalyst. The Selective Area Electron Diffraction (SAED) patterns by electron beam focusing on the crystalline nano-particles are exhibited in Figs. 3c and f, point out the distinct diffraction rings of the tetragonal phase of anatase TiO_2. The polycrystalline nature of the composite materials was confirmed by the SAED patterns.

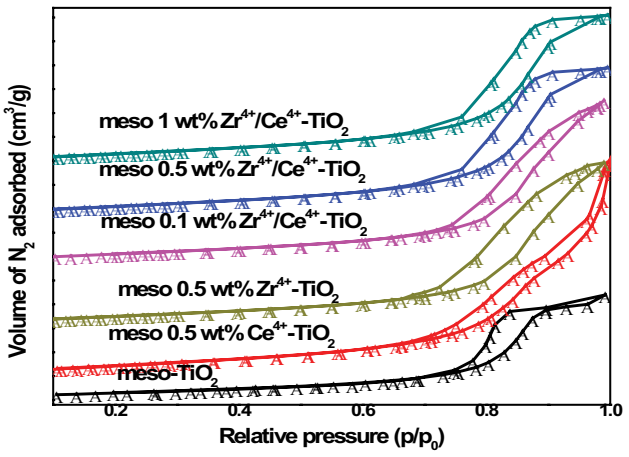

Fig. 2. N_2 sorption isotherms of meso-TiO_2, 0.5 wt.% Zr^{4+}-TiO_2, 0.5 wt.% Ce^{4+}-TiO_2, 0.1, 0.5 and 1 wt.% Zr^{4+}/Ce^{4+}-TiO_2.

XPS analysis was carried out to identify the chemical oxidation states of the elements in 0.5 wt.% Zr^{4+}/Ce^{4+}-TiO_2 catalyst. As shown in Fig. 4a, the XPS survey scan spectrum clearly indicates the existence of Ti, O, C, Ce and Zr elements in 0.5 wt.% Zr^{4+}/Ce^{4+}-TiO_2 nanocomposites. The carbon atom could be attributed to the extrinsic C-based impurity, and the peak at 284.3 eV was the binding energy of C 1s taken as reference. The binding energy around 470 eV for the Ti 2p state was exhibited in Fig. 4b. The peak situated at 464.59 eV matches Ti $2p_{1/2}$ then another one peak situated at 458.91 eV was allocated to Ti $2p_{3/2}$ this confirmed the tetragonal arrangement of Ti^{4+} [36]. The splitting between the Ti $2p_{1/2}$ and Ti $2p_{3/2}$ is 5.68 eV, also confirms the state of Ti^{4+} ion [37,38]. The peak at 529.49 eV for O1s core level (Fig. 4c) can be ascribed to TiO_2 lattice oxygen, whereas the Ti–OH surface OH groups confirmed by a peak at 532.0 eV [39,40]. The photoelectron spectra of Ce 3d is exhibited in Fig. 4d. The spectra of Ce 3d can be allocated to be $3d_{3/2}$ spin-orbit states as specified u and $3d_{5/2}$ states as specified v. The doublet u‴/v‴ is appropriate to elementary photoemission from Ce^{4+} - O_2. The doublets u/v, as well as, u″/v″ are shakedown characteristics resulting from the shift of 1 or 2 electrons from completely filled O_2p orbital to the empty or unfilled Ce 4f orbital. The doublet u′/v′ is suitable for the Ce^{3+} cations photoemission. The existence of doublet u′/v′ peaks in the spectrum shows that the Ce^{4+}-TiO_2 samples contain some O_2 vacancies and cerium ion as partially

Table 1
Textural and physicochemical properties of meso-TiO_2, 0.5 wt.% Zr^{4+}-TiO_2, 0.5 wt.% Ce^{4+}-TiO_2, 0.1, 0.5 and 1 wt.% Zr^{4+}/Ce^{4+}-TiO_2

Photocatalysts	Particle size (nm)	Bandgap energy (eV)	Specific surface area (m^2/g)	Pore diameter (nm)	Pore volume (cm^3/g)
Meso-TiO_2	11.8	3.13	80	9.8	0.40
0.5 wt.% Zr^{4+}-TiO_2	10.6	3.0	87	10.7	0.47
0.5 wt.% Ce^{4+}-TiO_2	10.2	2.93	90	11.8	0.51
0.1 wt.% Zr^{4+}/Ce^{4+}-TiO_2	9.4	2.73	92	12.2	0.53
0.5 wt.% Zr^{4+}/Ce^{4+}-TiO_2	8.3	2.49	98	12.9	0.55
1 wt.% Zr^{4+}/Ce^{4+}-TiO_2	7.5	2.40	96	11.7	0.57

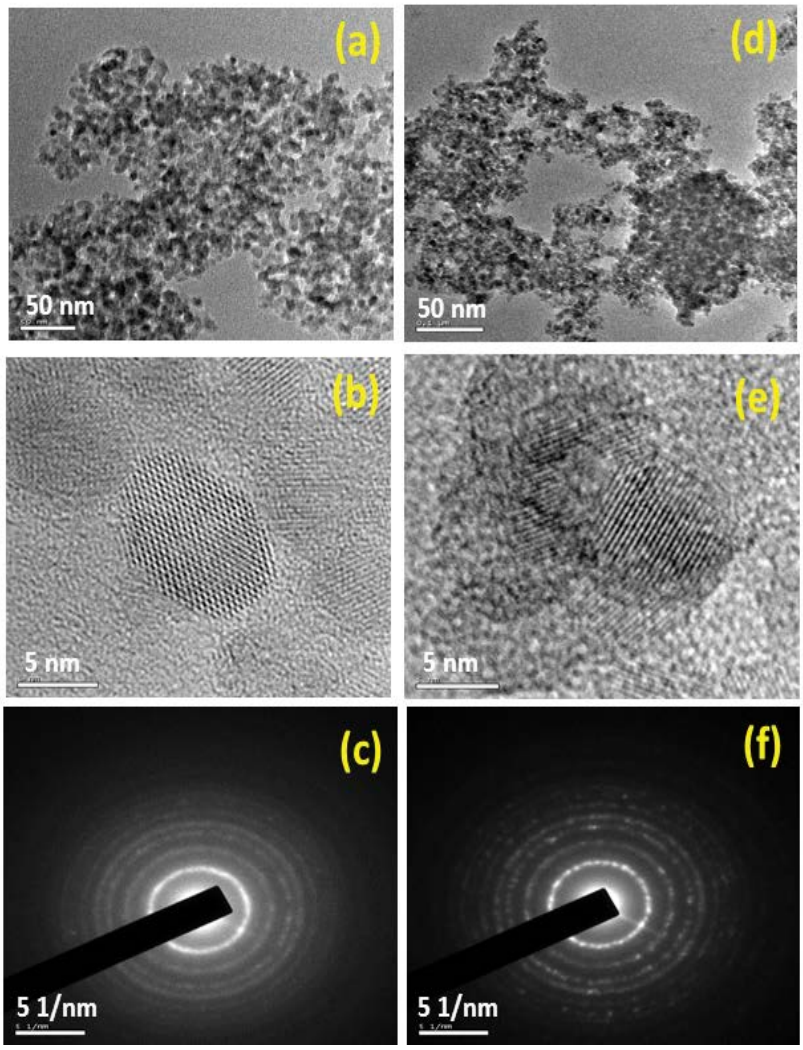

Fig. 3. HRTEM images (a) meso-TiO_2, (b) magnified image of meso-TiO_2, (c) SAED pattern of meso-TiO_2, (d) 0.5 wt.% Zr^{4+}/Ce^{4+}-TiO_2, (e) magnified image of 0.5 wt.% Zr^{4+}/Ce^{4+}-TiO_2, and (f) SAED pattern of 0.5 wt.% Zr^{4+}/Ce^{4+}-TiO_2.

reduced Ce^{3+} state. The incomplete photoreduction of Ce^{4+} in the time of XPS analysis is a notorious fact in the literature [25,41–43]. Thus, the Ce 3d spectrum of the Ce^{4+}-TiO_2 concludes that the presence of Ce^{4+} oxidation states. The Zr 3d XPS spectrum is shown in (Fig. 4e). The Zr^{4+} of zirconium was confirmed by the spectral lines at 183.3 eV and 185.5 eV matching respectively to the Zr $3d_{5/2}$ and Zr $3d_{3/2}$ [24]. The splitting between the Zr $3d_{5/2}$ and Zr $3d_{3/2}$ is 2.2 eV. The XPS spectra results conclude that cerium and zirconium ions exist as +4 oxidation state in TiO_2 photocatalyst.

The differential reflectance spectroscopy-ultraviolet-visible absorption spectrum of bare meso-TiO_2 and doped meso-TiO_2 are exhibited in Fig. 5. Commencement of absorption lines for meso-TiO_2, 0.5 wt.% Zr^{4+}-TiO_2, 0.5 wt.% Ce^{4+}-TiO_2, 0.1, 0.5 and 1 wt.% Zr^{4+}/Ce^{4+}-TiO_2 were obtained at 396, 413, 423, 454, 497 and 516 nm respectively. The values of bandgap energy determined using Kubelka–Munk equation $E_g = 1{,}240/\lambda$ (λ is the wavelength in nm) based on the beginning of absorbance were established to be 3.13, 3.0, 2.93, 2.73, 2.49 and 2.40 eV for bare meso-TiO_2, 0.5 wt.% Zr^{4+}-TiO_2, 0.5 wt.% Ce^{4+}-TiO_2, 0.1, 0.5 and 1 wt.% Zr^{4+}/Ce^{4+}-TiO_2. Zirconium and cerium co-doping on TiO_2 caused a redshift in the absorption edge of TiO_2 from 413 to 516 nm. The redshift within TiO_2 revealed the existence of Zr–O–Ti and Ti–O–Ce bonds [44]. The redshift may be caused due to the fresh energy level produced within the bandgap, which diminished the TiO_2 bandgap. All the synthesized nanocomposite materials apart from meso-TiO_2 proved the proper red shift in optical absorption spectroscopy studies with energies of bandgap varies from 3.1 to 2.45 eV, which is expected to induce visible light absorption TiO_2.

The FTIR spectra of bare meso-TiO_2 and doped TiO_2 photocatalysts are shown in Fig. 6. All the photocatalysts exhibit a wide absorption band between 3,300 and 3,450 cm^{-1} that corresponds to the stretching vibration of OH groups. The absorption band peaks at 1,627 and 2,365 cm^{-1} are associated with the bending vibration peaks of OH groups and surface adsorbed CO_2 respectively. The large absorption band detected at around 550–750 cm^{-1} for all the photocatalysts corresponds to the characteristic vibrations of

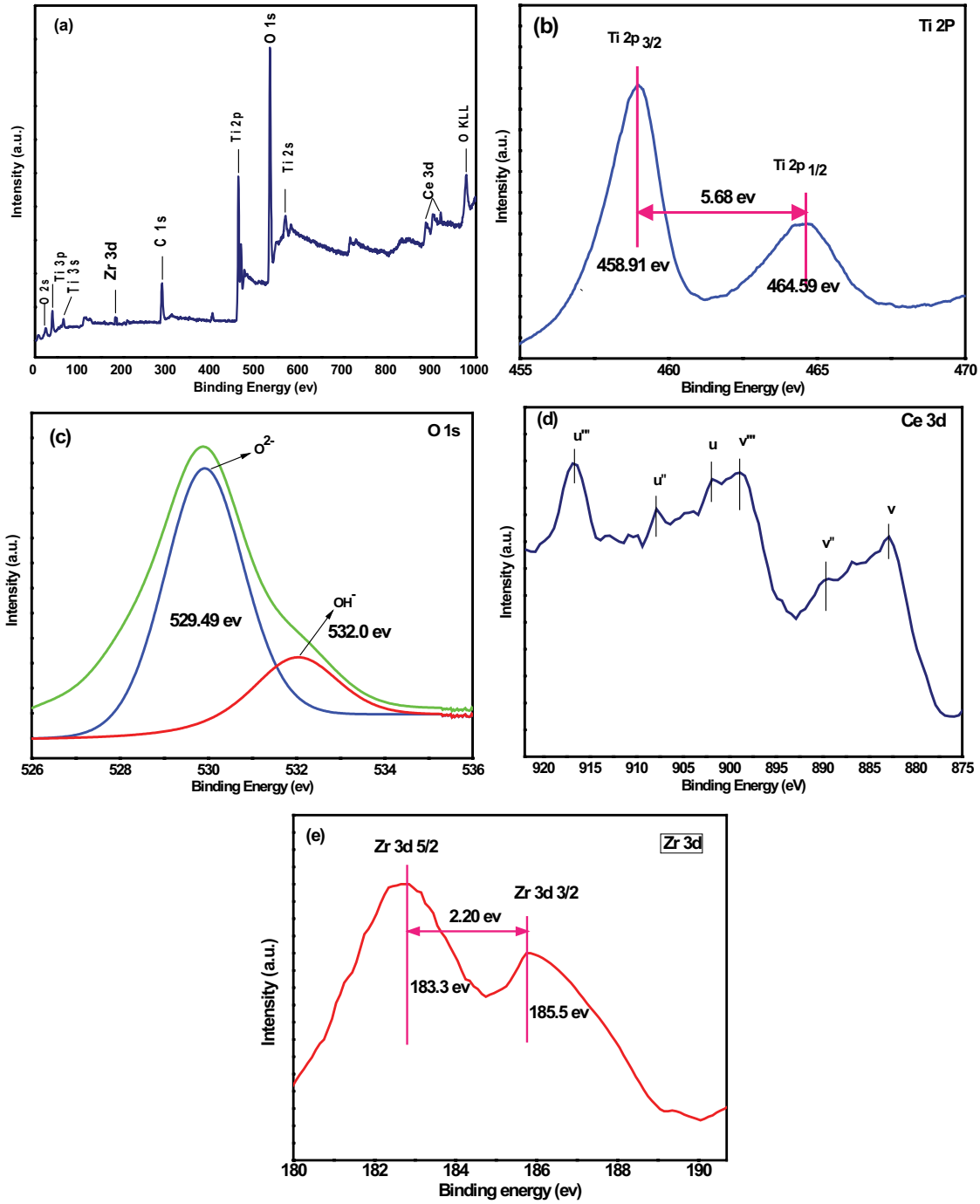

Fig. 4. XPS spectra of meso-0.5 wt.% Zr^{4+}/Ce^{4+}-TiO_2 (a) survey, (b) Ti 2p, (c) O 1s, (d) Ce 3d, and (e) Zr 3d.

TiO_2 [45]. The nonexistence of CH_2 bending and stretching vibrations in all calcined catalytic materials specify the complete elimination of solvent (alcohol) and polymer template at 400°C.

3.2. Evaluation of photocatalytic activity

The photocatalytic rates of meso-TiO_2, 0.5 wt.% Zr^{4+}-TiO_2, 0.5 wt.% Ce^{4+}-TiO_2, 0.1, 0.5 and 1 wt.% Zr^{4+}/Ce^{4+}-TiO_2 photocatalysts were estimated for the degradation of 2,4-dinitrophenol using irradiation of visible light beyond 400 nm are calculated and plotted against metal ions loading as shown in Fig. 7. The speed of photodegradation of 2,4-DNP under visible light was established to be extremely low on bare meso titania due to lack of absorption of visible light by TiO_2. The photocatalytic performance of TiO_2 increases with an increase in metal ion loading and shows a maximum at 0.5 wt.% and then decreases. The

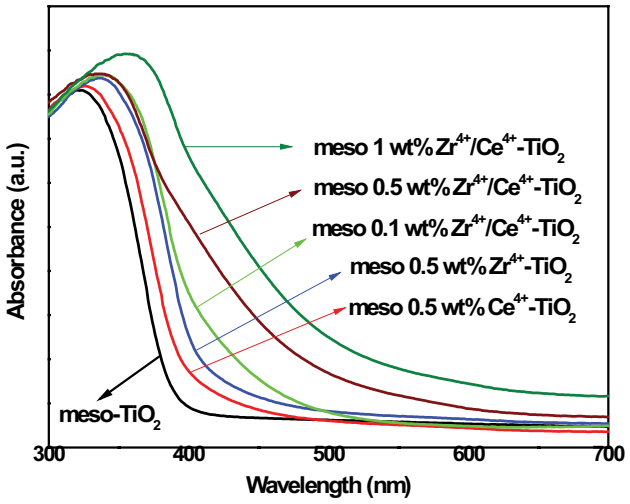

Fig. 5. Differential reflectance spectroscopy-ultraviolet spectra of meso-TiO_2, 0.5 wt.% Zr^{4+}-TiO_2, 0.5 wt.% Ce^{4+}-TiO_2, 0.1, 0.5 and 1 wt.% Zr^{4+}/Ce^{4+}-TiO_2.

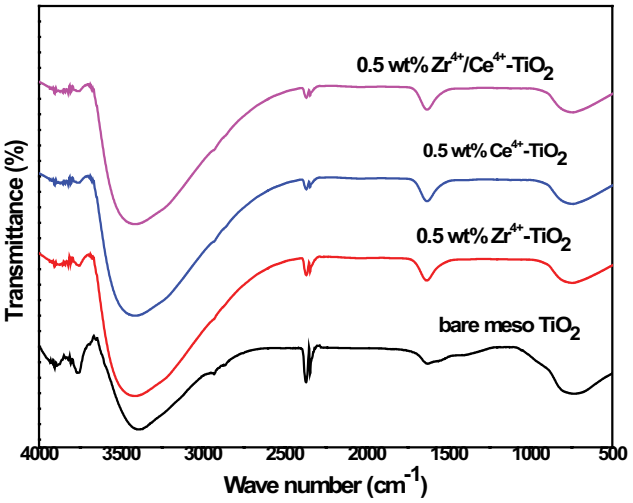

Fig. 6. FTIR spectra of bare meso-TiO_2, 0.5 wt.% Zr^{4+}-TiO_2, 0.5 wt.% Ce^{4+}-TiO_2, 0.5 wt.% Zr^{4+}/Ce^{4+}-TiO_2.

band-gap narrowing and improved visible light absorption of TiO_2 by co-doping (Zr and Ce) lead to enhanced photocatalytic activity of the TiO_2 under visible light.

Among the different wt.% loading of Zr^{4+} and Ce^{4+}, 0.5 wt.% of Zr^{4+}/Ce^{4+} on TiO_2 exhibited much enhanced photocatalytic activity towards 2,4-DNP, this could be recognized to the increase in surface area with large pore diameter. These textural parameters improve the adsorption of 2,4-DNP molecules into the pores of TiO_2. The rate of degradation increased with an increase of dopant concentration up to 0.5 wt.% of Zr^{4+} and 0.5 wt.% of Ce^{4+} on meso-TiO_2. Since the surface area decreases with an increase in dopant concentration, the degradation rate decreased. The superior catalytic activity of 0.5 wt.% Zr^{4+}/Ce^{4+}-TiO_2 photocatalytic material was confirmed by the analysis of the TOC. The analysis of TOC was carried

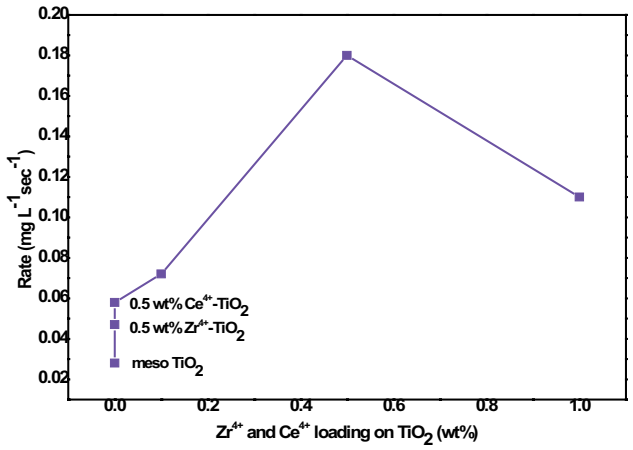

Fig. 7. Degradation rates of 2,4-dinitrophenol with meso-TiO_2, 0.5 wt.% Zr^{4+}-TiO_2, 0.5 wt.% Ce^{4+}-TiO_2, 0.1, 0.5 and 1 wt.% Zr^{4+}/Ce^{4+}-TiO_2.

out and the plot of TOC vs. irradiation time is exhibited in Fig. 8. The photodegradation of 2,4-DNP was established to be a higher rate at 0.5 wt.% Zr^{4+}/Ce^{4+}-TiO_2 photocatalyst compared with meso-TiO_2 and doped meso-TiO_2.

3.3. Photocatalytic mechanism

The proposed mechanism for photocatalysis on Zr^{4+}/Ce^{4+}-TiO_2 is shown in Fig. 9. It is well recognized that the doping of zirconium and cerium ions on TiO_2 plays a significant role as a visible-light activated photocatalyst [46]. When the co-doped TiO_2 irradiates by visible light, the electrons and holes are generated and are assisted by the degradation of pollutants through photocatalytic redox reactions. Since the bandgap of co-doped TiO_2 photocatalysts is reduced, all TiO_2 are activated in a visible light region. Since the photoexcited electrons are caught by Ce^{4+} ions, the photogenerated negative electrons and positive holes were efficiently separated on the surface of the TiO_2 to increase the electron-hole lifetime. On zirconium doping, the photo-generated electrons are likely to build up the energy level at the surface state and photo-generated holes are captured together on the surface of the TiO_2 valence band. Consequently, the adsorbed hydroxyl groups on the surface of TiO_2 were also increased. This was also disclosed by XPS analysis where the spectral lines at 532.0 eV are allocated to Ti–OH surface OH^- groups. During the photocatalytic degradation, 2,4-DNP pollutant adsorbed on the alive exterior sites of doped TiO_2 and readily oxidized by photogenerated positive holes into $^{\bullet}OH$ radicals. Therefore, the electron-hole recombination was suppressed by the introduction of Ce^{4+} ions into the TiO_2 lattice.

Cerium doping creates an impurity energy level within the bandgap of TiO_2. Therefore, the agitated electrons at the conduction band or an impurity energy level can diminish Ce^{4+} to Ce^{3+} ions in the presence of visible light irradiation. The CB of TiO_2 or the impurity energy level is extra negative compared to the reduction potential of Ce^{4+} ion to Ce^{3+} ion (+1.61 eV). The electrons captured in the Ce^{4+} ionic sites can

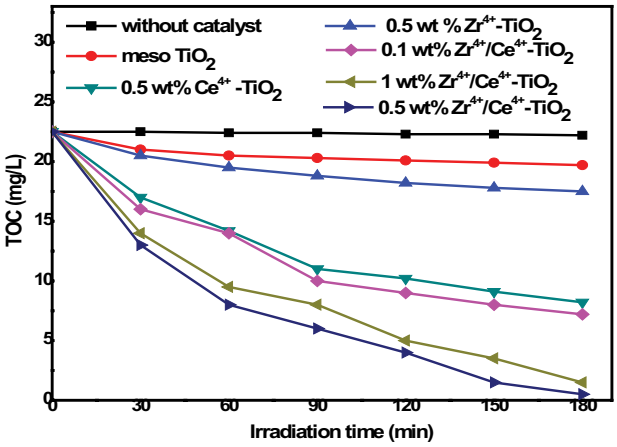

Fig. 8. Photocatalytic degradation of 2,4-dinitrophenol with bare meso-TiO_2, 0.5 wt.% Zr^{4+}-TiO_2, 0.5 wt.% Ce^{4+}-TiO_2, 0.1, 0.5 and 1 wt.% Zr^{4+}/Ce^{4+}-TiO_2.

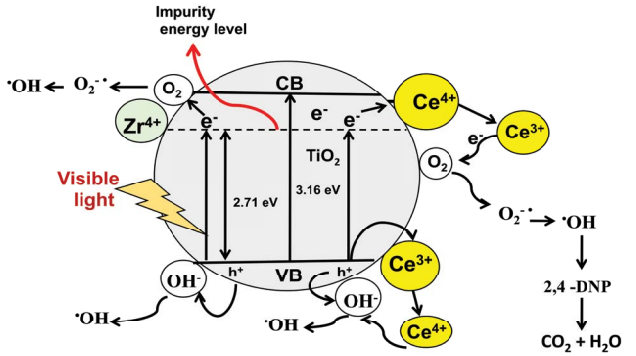

Fig. 9. Proposed mechanism for photocatalysis on meso-Zr^{4+}/Ce^{4+}-TiO_2.

be simply shifted to adsorbed O_2 molecules on the surface of Ce doped TiO_2 photocatalysts to formation oxidizing species ($O_2^{-\bullet}$). Also, VB of TiO_2 has a probable of +2.9 V this is more positive compared to the oxidation potential of the Ce^{3+} ion to Ce^{4+} ion (–1.61 eV). The valence band positive holes can be oxidized Ce^{3+} ion to Ce^{4+} ion. These oxidized Ce^{4+} ions can consequently shift the holes to OH groups, which create a more number of extremely active hydroxyl (•OH) radicals [47]. The Ce^{3+} and Ce^{4+} coexisting in ZrO_2/CeO_2-TiO_2 influence the photoreactivity by withholding the electron–hole pair recombination time. However, the positive holes and excited electrons can be captured by Ce^{3+} ion and Ce^{4+} ion respectively.

The valence band in the TiO_2 has an affinity to undergo further reduction, therefore the photogenerated positive holes can simply oxidize the adsorbed hydroxyl group and formation of •OH radicals, which was a potent oxidizing agent to degradation of 2,4-DNP. The formation of a large number of $O_2^{-\bullet}$ and •OH by zirconium and cerium ultimately enhanced the photocatalytic activity of TiO_2 utilizing visible light irradiation.

4. Conclusion

In this study, Zr^{4+}/Ce^{4+}-TiO_2 nanocatalysts were prepared by sol–gel technique using Pluronic P123 as structure-directing template. The resulting co-doped TiO_2 photocatalysts showed extended absorbance in the visible light region and subsequently reduced the bandgap of TiO_2 in comparison with bare meso-TiO_2. The zirconium and cerium co-doped photocatalytic materials proved better photocatalytic activity than meso-TiO_2, Zr^{4+}-TiO_2 and Ce^{4+}-TiO_2 under visible light irradiation. Among all the prepared photocatalytic materials with different dopant concentration, 0.5 wt.% co-doped TiO_2 nanocatalyst proved the maximum photocatalytic activity due to the enhanced surface area with large pore diameter. The large mesopores provide more pathways for a 2,4-DNP pollutants to easily access the active sites inside the pores of TiO_2. Ce^{4+} is the best electron scavenger and reduces the adsorbed O_2 molecules to produce superoxide anion radicals and enhanced the photocatalytic performance by preventing the electron-hole pair recombination. The incorporation of Zr^{4+} in TiO_2 led to small particle size, large surface area and also led to form more electron capture traps, which contribute to high separation efficiency of photogenerated carriers. Co-doped meso-TiO_2 ultimately enhanced the photocatalytic activity by the synergistic effect of trapping, suppressing the electron-hole pair recombination and improved light absorption in the visible light region.

References

[1] S. Ahmed, M.G. Rasul, W.N. Martens, R. Brown, M.A. Hashib, Heterogeneous photocatalytic degradation of phenols in wastewater: a review on current status and developments, Desalination, 261 (2010) 3–18.
[2] M.N. Chong, B. Jin, C.W.K. Chow, C. Saint, Recent developments in photocatalytic water treatment technology: a review, Water Res., 44 (2010) 2997–3027.
[3] W.Y. Teoh, R. Amal, L. Madler, S.E. Pratsnis, TiO_2 nanotube deposited in the pores of expanded graphite by microwave irradiation, Catal. Today, 120 (2007) 203–213.
[4] W.Y. Choi, Pure and modified TiO_2 photocatalysts and their environmental applications, Catal. Surv. Asia, 10 (2006) 16–28.
[5] J.H. Pan, X.W. Zhang, A.J.H. Du, D.D. Sun, J.O. Leckie, Self-etching reconstruction of hierarchically mesoporous F-TiO_2 hollow microspherical photocatalyst for concurrent membrane water purifications, J. Am. Chem. Soc., 130 (2008) 11256–11257.
[6] G. Veréb, L. Manczinger, A. Oszkó, A. Sienkiewicz, L. Forró, K. Mogyorósi, A. Dombi, K. Hernádi, Highly efficient bacteria inactivation and phenol degradation by visible light irradiated iodine doped TiO_2, Appl. Catal., B, 129 (2013) 194–201.
[7] K.L. Lv, B. Cheng, J.G. Yu, G. Liu, Fluorine ions-mediated morphology control of anatase TiO_2 with enhanced photocatalytic activity, Phys. Chem. Chem. Phys., 14 (2012) 5349–5362.
[8] H.M. Zhang, X. Quan, S. Chen, H.M. Zhao, Fabrication and characterization of silica/titania nanotubes composite membrane with photocatalytic capability, Environ. Sci. Technol., 40 (2006) 6104–6109.
[9] P. Vijayan, C. Mahendiran, C. Suresh, K. Shanthi, Photocatalytic activity of iron doped nanocrystalline titania for the oxidative degradation of 2,4,6-trichlorophenol, Catal. Today, 141 (2009) 220–224.
[10] B. Palanisamy, C.M. Babu, B. Sundaravel, S. Anandan, V. Murugesan, Sol–gel synthesis of mesoporous mixed Fe_2O_3/TiO_2 photocatalyst: application for degradation of 4-chlorophenol, J. Hazard. Mater., 252 (2013) 233–242.

[11] Y.M. Cho, W.Y. Choi, C.-H. Lee, T.W. Hyeon, H.-I. Lee, Visible light-induced degradation of carbon tetrachloride on dye-sensitized TiO_2, Environ. Sci. Technol., 35 (2001) 966–970.
[12] Y. Xie, S.H. Heo, Y.N. Kim, S.H. Yoo, S.O. Cho, Synthesis and visible-light-induced catalytic activity of Ag_2S-coupled TiO_2 nanoparticles and nanowires, Nanotechnology, 21 (2010) 015703.
[13] A. Di Paola, L. Palmisano, A.M. Venezia, V. Augugliaro, Coupled semiconductor systems for photocatalysis. Preparation and characterization of polycrystalline mixed WO_3/WS_2 powders, J. Phys. Chem. B, 103 (1999) 8236–8244.
[14] Y.H. Ao, J.J. Xu, D.G. Fu, C.W. Yuan, A simple method to prepare N-doped titania hollow spheres with high photocatalytic activity under visible light, J. Hazard. Mater., 167 (2009) 413–417.
[15] Y. Wang, Y. Wang, Y.L. Meng, H.M. Ding, Y.K. Shan, X. Zhao, X.Z. Tang, A highly efficient visible-light-activated photocatalyst based on bismuth- and sulfur-codoped TiO_2, J. Phys. Chem. C, 112 (2008) 6620–6626.
[16] B. Malinowska, J. Walendziewski, D. Robert, J.W. Weber, M. Stolarski, The study of photocatalytic activities of titania and titania–silica aerogels, Appl. Catal., B, 46 (2003) 441–451.
[17] S.K. Poznyak, D.V. Talapin, A.I. Kulak, Structural, optical and photoelectrochemical properties of nanocrystalline TiO_2–In_2O_3 composite solids and films prepared by sol–gel method, J. Phys. Chem. B, 105 (2001) 4816–4823.
[18] Y. Cao, X.T. Zhang, W.S. Yang, H. Du, Y.B. Bai, T.J. Li, J.N. Yao, A bicomponent TiO_2/SnO_2 particulate film for photocatalysis, Chem. Mater., 12 (2000) 3445–3448.
[19] Z.F. Bian, J. Zhu, S.H. Wang, Y. Cao, X.F. Qian, H.X. Li, Self-assembly of active Bi_2O_3/TiO_2 visible photocatalyst with ordered mesoporous structure and highly crystallized anatase, J. Phys. Chem. C, 112 (2008) 6258–6262.
[20] B.M. Reddy, A. Khan, Recent advances on TiO_2-ZrO_2 mixed oxides as catalysts and catalyst supports, Catal. Rev. Sci. Eng., 47 (2005) 257–296.
[21] B.F. Gao, T.M. Lim, D.P. Subagio, T.-T. Lim, Zr-doped TiO_2 for enhanced photocatalytic degradation of bisphenol A, Appl. Catal., A, 375 (2010) 107–115.
[22] H.J. Liu, G.G. Liu, Q.X. Zhou, Preparation and characterization of Zr doped TiO_2 nanotube arrays on the titanium sheet and their enhanced photocatalytic activity, J. Solid State Chem., 182 (2009) 3238–3242.
[23] P. Goswami, J.N. Ganguli, Tuning the bandgap of mesoporous Zr-doped TiO_2 for effective degradation of pesticide quinalphos, Dalton Trans., 42 (2013) 14480–14490.
[24] L. Kumaresan, A. Prabhu, M. Palanichamy, E. Arumugam, V. Murugesan, Synthesis and characterization of Zr^{4+}, La^{3+} and Ce^{3+} doped mesoporous TiO_2: evaluation of their photocatalytic activity, J. Hazard. Mater., 186 (2011) 1183–1192.
[25] B. Palanisamy, C.M. Babu, B. Sundaravel, S. Anandan, V. Murugesan, Visible-light active mesoporous Ce incorporated TiO_2 for the degradation of 4-chlorophenol in aqueous solution, J. Nanosci. Nanotechnol., 13 (2013) 2573–2581.
[26] G.S. Li, D.Q. Zhang, J.C. Yu, Thermally stable ordered mesoporous CeO_2/TiO_2 visible-light photocatalysts, Phys. Chem. Chem. Phys., 11 (2009) 3775–3782.
[27] N. Zhao, M.-M. Yao, F. Li, F.-P. Lou, Microstructures and photocatalytic properties of Ag^+ and La^{3+} surface codoped TiO_2 films prepared by sol–gel method, J. Solid State Chem., 184 (2011) 2770–2775.
[28] X. Yang, F.Y. Ma, K.X. Li, Y.N. Guo, J.L. Hu, W. Li, M.X. Huo, Y.H. Guo, Mixed phase titania nanocomposite codoped with metallic silver and vanadium oxide: new efficient photocatalyst for dye degradation, J. Hazard. Mater., 175 (2010) 429–438.
[29] Z.-P. Liu, S.J. Jenkins, D.A. King, Role of nanostructured dual-oxide supports in enhanced catalytic activity: theory of CO oxidation over $Au/IrO_2/TiO_2$, Phys. Rev. Lett., 93 (2004) 156102, doi: 10.1103/PhysRevLett.93.156102.
[30] X. Zhang, Q.Q. Liu, Visible-light-induced degradation of formaldehyde over titania photocatalyst co-doped with nitrogen and nickel, Appl. Surf. Sci., 254 (2008) 4780–4785.
[31] M. Myilsamy, M. Mahalakshmi, V. Murugesan, N. Subha, Enhanced photocatalytic activity of nitrogen and indium co-doped mesoporous TiO_2 nanocomposites for the degradation of 2,4-dinitrophenol under visible light, Appl. Surf. Sci., 342 (2015) 1–10.
[32] G.D. Yang, Z.F. Yan, T.C. Xiao, Preparation and characterization of $SnO_2/ZnO/TiO_2$ composite semiconductor with enhanced photocatalytic activity, Appl. Surf. Sci., 258 (2012) 8704–8712.
[33] P. Zhang, Y.L. Yu, E.J. Wang, J.S. Wang, J.H. Yao, Y. Cao, Structure of nitrogen and zirconium co-doped titania with enhanced visible-light photocatalytic activity, ACS Appl. Mater. Interfaces, 6 (2014) 4622–4629.
[34] L. Kumaresan, A. Prabhu, M. Palanichamy, V. Murugesan, Synthesis of mesoporous TiO_2 in aqueous alcoholic medium and evaluation of its photocatalytic activity, Mater. Chem. Phys., 126 (2011) 445–452.
[35] S.P. Tandon, J.P. Gupta, Measurement of forbidden energy gap of semiconductors by diffuse reflectance technique, Phys. Status Solidi B, 38 (1970) 363–367.
[36] J.F. Moulder, W.F. Stickle, P.E. Sobol, K.D. Bomben, Handbook of X-Ray Photoelectron Spectroscopy, Physical Electronics Division, Perkin-Elmer Corp., Eden Prairie, MN, 1992.
[37] H.M. Yadav, T.V. Kolekar, S.H. Pawar, J.-S. Kim, Enhanced photocatalytic inactivation of bacteria on Fe-containing TiO_2 nanoparticles under fluorescent light, J. Mater. Sci.: Mater. Med., 27 (2016) 57, https://doi.org/10.1007/s10856-016-5675-8.
[38] H.M. Yadav, S.V. Otari, R.A. Bohara, S.S. Mali, S.H. Pawar, S.D. Delekar, Synthesis and visible light photocatalytic antibacterial activity of nickel-doped TiO_2 nanoparticles against gram-positive and gram-negative bacteria, J. Photochem. Photobiol., A, 294 (2014) 130–136.
[39] H.M. Yadav, S.V. Otari, V.B. Koli, S.S. Mali, C.K. Hong, S.H. Pawar, S.D. Delekar, Preparation and characterization of copper-doped anatase TiO_2 nanoparticles with visible light photocatalytic antibacterial activity, J. Photochem. Photobiol., A, 280 (2014) 32–38.
[40] Y.-H. Xu, H.-R. Chen, Z.-X. Zeng, B. Lei, Investigation on mechanism of photocatalytic activity enhancement of nanometer cerium-doped titania, Appl. Surf. Sci., 252 (2006) 8565–8570.
[41] Y.-L. Kuo, C. Lee, Y.-S. Chen, H. Liang, Gadolinia-doped ceria films deposited by RF reactive magnetron sputtering, Solid State Ionics, 180 (2009) 1421–1428.
[42] E. Beche, P. Charvin, D. Perarnau, S. Abanades, G. Flamant, Ce 3d XPS investigation of cerium oxides and mixed cerium oxide ($Ce_xTi_yO_z$), Surf. Interface Anal., 40 (2008) 264–267.
[43] C. Karunakaran, P. Gomathisankar, G. Manikandan, Preparation and characterization of antimicrobial Ce-doped ZnO nanoparticles for photocatalytic detoxification of cyanide, Mater. Chem. Phys., 123 (2010) 585–594.
[44] M. Myilsamy, V. Murugesan, M. Mahalakshmi, Indium and cerium co-doped mesoporous TiO_2 nanocomposites with enhanced visible light photocatalytic activity, Appl. Catal., A, 492 (2015) 212–222.
[45] Y.F. Zhu, L. Zhang, C. Gao, L. Cao, The synthesis of nanosized TiO_2 powder using a sol–gel method with $TiCl_4$ as a precursor, J. Mater. Sci., 35 (2000) 4049–4054.
[46] M.H. Li, S.J. Zhang, L. Lv, M.S. Wang, W.M. Zhang, B.C. Pan, A thermally stable mesoporous ZrO_2–CeO_2–TiO_2 visible light photocatalyst, Chem. Eng. J., 229 (2013) 118–125.
[47] G. Magesh, B. Viswanathan, R.P. Viswanath, T.K. Varadarajan, Photocatalytic behavior of CeO_2-TiO_2 system for the degradation of methylene blue, Indian J. Chem., 48 (2009) 480–488.